EurJIC European Journal of Inorganic Chemistry

ChemPubSoc Europe

FULL PAPER

DOI:10.1002/ejic.201300308

Connecting [4Fe–4S] Clusters and Hemes – Towards Modeling the Active Site of Sulfite Reductase

Deidra L. Gerlach,[a] Dimitri Coucouvanis,*[a] and Nicolai Lehnert*[a]

Keywords: Iron–sulfur cluster / Zinc / Porphyrinoids / Bioinorganic chemistry / Enzyme mimics / Bridging ligands

In this paper, we present a new design for biologically *inspired* models for the active site of assimilatory sulfite and nitrite reductases (aSIR and aNIR), which consists of a siroheme that is directly linked to a [4Fe–4S] cubane cluster. The individual components used here to construct this model are a site-differentiated [4Fe–4S] cluster, a bifunctional bridging ligand, and a metalloporphyrin. We have prepared two new site-differentiated clusters, $[Fe_4S_4(TriS)(SPy)]$ and $[Fe_4S_4(TriS)(SEtIm)]$, which contain pyridine and imidazole linkers for the binding to a metalloporphyrin, and characterized these compounds, using **UV/Vis**, IR, and ^{1}H-NMR spectroscopy, cyclic voltammetry (CV), and mass spectrometry. Titration experiments where then performed by using [Zn(TPP)] (TPP^{2-} = *meso*-tetraphenylporphyrin dianion) and corresponding fluorinated derivatives to find the best [4Fe–4S]–heme combination for an optimal binding of the two components in solution. *Excitingly, our results demonstrate the formation of the desired [4Fe–4S]–heme catalytic arrays in solution with high specificity.* The best combination of cubane cluster and metalloporphyrin for future catalyst development corresponds to the complex $(Bu_4N)_2[M(To\text{-}F_2PP)–\{Fe_4S_4(TriS)(SEtIm)\}]$ {To-F_2PP^{2-} = *meso*-tetra(*ortho*-difluorophenyl)porphyrin dianion}. The binding between these components with M = Zn^{2+} was further confirmed by CV. Thus, we have created a new type of biologically inspired model system for the aSIR and aNIR active site that leads to a robust attachment of the individual components in solution.

Introduction

Ferredoxins are typically utilized in biological systems in electron transfer chains; it is rare to find ferredoxins of the [4Fe–4S] variety in the active sites of enzymes covalently linked to a catalytic site.[1] Only three examples of such metalloproteins are known. In these cases, the ferredoxin is covalently bound to the catalytic site through a cysteine thiolate or a sulfide bridge for the purpose of fast electron transfer to the catalytic metal center, which is responsible for substrate binding and reduction. Each of these three classes of metalloproteins has a very specialized role in nature, and all of them are part of anaerobic processes. The iron–iron hydrogenase catalyses the reversible reduction of protons to hydrogen at a sulfide-bridged diiron cluster known as the H cluster.[2] Acetyl CoA synthase catalyses the synthesis of acetyl coenzyme A by the initial generation of an acetyl group from the reduction of CO_2 and the subsequent transfer of a methyl group at the cysteinato-bridged Ni(Cu)–Ni cluster, the A-cluster.[3] Sulfite and nitrite reductase hemoproteins (SIR and NIR) catalyse the reduction of sulfite and nitrite to sulfide and ammonia, respectively, at a siroheme.[4] Although heme and iron–sulfur clusters are found in many metalloproteins, where they serve as electron-transfer and catalytic sites, SIR and NIR are unique in that they are the only known metalloenzymes that incorporate a bridged heme–ferrodoxin center in the active site.

The reduction power of assimilatory SIR and NIR (aSIR and aNIR) is what makes these heme proteins so interesting, as they can reduce the substrate by an unprecedented six electrons, before releasing the final product.[4] The closely related dissimilatory sulfite and nitrite reductases catalyse the reduction of sulfite and nitrite in two-electron steps for the purpose of detoxification. Overall, the key components of the active site of SIRs and NIRs are a catalytic heme bound to a ferredoxin electron reservoir with an electron-conducting bridge that connects them.[5] The reduction potentials of the siroheme and the iron–sulfur cluster found in aSIR of *E. coli* are –340 and –405 mV, respectively.[5] The active sites of the assimilatory and dissimilatory varieties of the SIR and NIR enzymes are essentially identical, and the most significant differences are observed in the secondary structures of the proteins and in the substrate channels. Because of their closely related active sites, sulfite is reduced by NIR and nitrite is reduced by SIR but not at the full catalytic rate for the natural substrate.[6] It can be inferred that the reduction of the substrate occurs generally in two-electron increments to release a water molecule (for every two electrons transferred), as proposed for

[a] Department of Chemistry, University of Michigan, 930 N University, Ann Arbor, MI 48109
E-mail: lehnertn@umich.edu

Supporting information for this article is available on the WWW under http://dx.doi.org/10.1002/ejic.201300308.

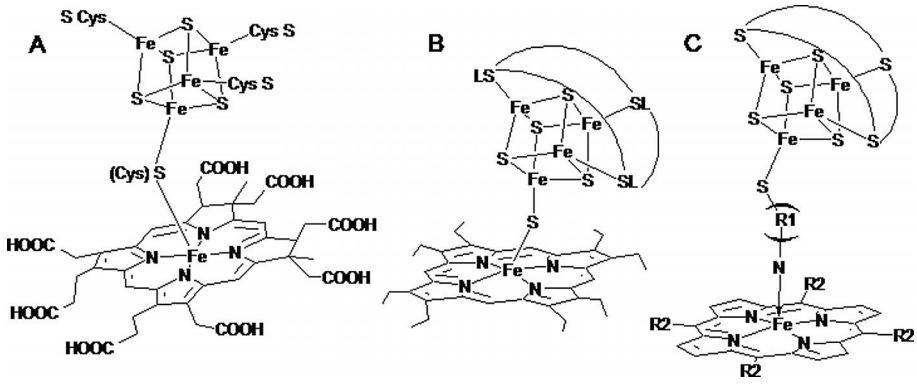

Scheme 1. The active site of SIR and NIR (A); a biomimetic model complex by Holm and co-workers (B); biologically inspired complex design applied here (C).

the dissimilatory variety.[7] Most recent research has shown the importance of the protein residues in the substrate binding pocket of the active site of aSIR and provides strong evidence for a "push–pull" mechanism, where the proton and the electron transfer to the substrate are linked.[8] Substrate reduction occurs by binding at the distal side of the siroheme in the ferrous state, and protons are supplied with the aid of the carboxylic groups of the siroheme and of ordered waters in the active-site pocket.[9] Although the exact sequence of electron transfer between the [4Fe–4S] cluster and the siroheme of the active site is not known, it has been shown that both the cluster and the heme are reduced by one electron each in the fully reduced state of the enzyme.[10]

In previous model studies by Holm and co-workers, the assembly of a biomimetic model complex for SIR consisting of a ferric octaethylporphyrin bridged by sulfide to the LS_3 site-differentiated [4Fe–4S] cubane cluster was reported. The formation of the bridged unit in solution was demonstrated by spin delocalization to the heme and the LS_3 ligand, as determined by ^1H NMR and Mössbauer spectroscopy.[11] This model complex could not be isolated, but it could be doubly reduced in solution in two one-electron steps. No further comments on the stability or the potential substrate reduction were made in the original report. Unlike the enzyme, the model complex does not have a support structure for stabilizing the sulfido link between the [4Fe–4S] cluster and the heme. This link is susceptible to dissociation in polar solvents and in the presence of protons, which on the other hand are necessary to emulate the reactivity of SIR and NIR. Because of the limitations in stability of a sulfido bridge between the catalytic and the electron-reservoir moieties in the original SIR and NIR models, we have chosen a different approach to incorporate the chemical functions of the active site, utilizing a bridge that is more robust (and less biomimetic) than a single sulfide anion. In this paper, we present our new biologically *inspired* SIR and NIR model complex design comprised of a metalloporphyrin bridged by a small organic ligand to a site-differentiated [4Fe–4S] cubane cluster, which is ligated by an encapsulating ligand (Scheme 1). The small bridging ligand is designed to preferentially bind to the [4Fe–4S] cluster through a thiolate and to the axial coordination site of the metalloporphyrin through a pyridine or imidazole group. The bridging ligands employed here are *para*-thiopyridine and 1-ethylthioimidazole. First, we synthesized site-differentiated [4Fe–4S] clusters with these bridging ligands. Subsequently, titration data monitored by UV/Vis absorption spectroscopy and cyclic voltammetry (CV) clearly show the assembly of the full catalytic unit in solution. We further tested and identified the most appropriate heme and the best organic bridge for generating the most robust linkage between the catalytic and the electron-reservoir components of our model complex.

Results and Discussion

Cluster Syntheses and Functionalization

Iron–sulfur cubane clusters are easily prepared in a one-pot, self-assembly reaction under anaerobic conditions.[12] Halides, thiolates, and strong σ-donors, such as imines and phosphanes, are the preferred ligands of iron–sulfur clusters. Because each [4Fe–4S] cluster typically ligates an anionic ligand at each iron corner of the cubane, a large encapsulating ligand was first applied to the tetrakis(ethylthiolato) cluster to leave only one corner of the cluster exposed and, in this way, to allow for only one heme to bind to each cubane (Scheme 2). The $TriSH_3$ ligand was first designed by Pohl and co-workers, and it was chosen here for its functionality and the ease of its synthesis.[13] The ligand exchange is initiated by the protonation of ethylthiolate by the incoming thiol, and it is driven by the evaporation of the volatile ethanethiol in the evacuated reaction flask. The resulting site-differentiated cubane cluster has one remaining ethylthiolato ligand, which is subsequently replaced by the bridging ligand. This synthetic route is presented in Scheme 2. The bridging ligand is designed to have an anionic thiolate for preferential binding to the [4Fe–4S] cluster and a neutral pyridine or imidazole for binding to the axial position of the metalloporphyrin. A neutral N-donor ligand is preferred for the binding to the heme to minimize the propensity of ligand dissociation, when the metal goes through oxidation state changes: the iron center of the ulti-

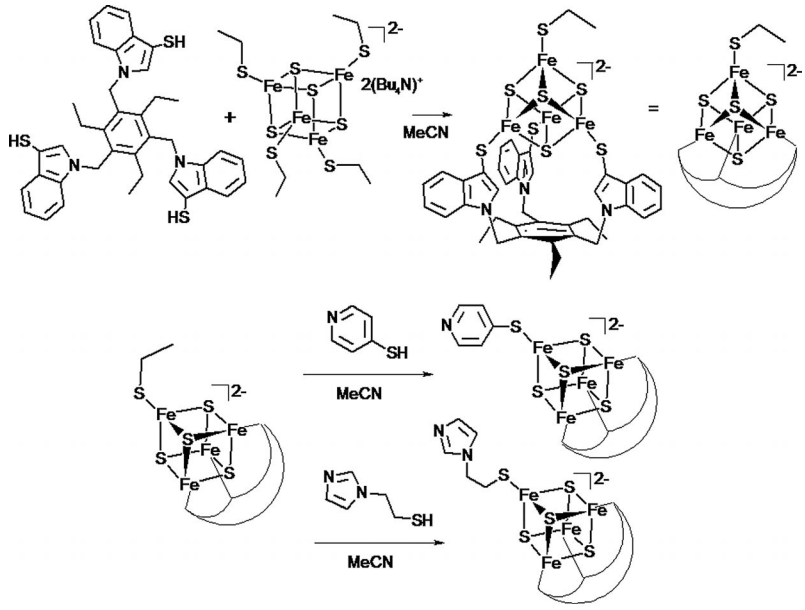

Scheme 2. Synthetic scheme for the site-differentiated [4Fe–4S] cubane clusters with bound pyridine and imidazole linkers.

mately desired iron porphyrin is expected to cycle through the ferric and ferrous oxidation state during substrate binding and reduction; hence, a neutral N-donor ligand is advantageous for maintaining the structural connection to the [4Fe–4S] cluster.

The ^{1}H-NMR spectra of the [4Fe–4S] cubane cluster are broad, and significant paramagnetic shifts are observed for the protons closest to the irons. Identifying the peaks for the new bridging ligands in $(Bu_4N)_2[Fe_4S_4(TriS)(SPy)]$ and $(Bu_4N)_2[Fe_4S_4(TriS)(SEtIm)]$ is difficult because of the significant broadening of these peaks. We observed broad signals for the ligand SPy at δ = 8.83 and 6.10 ppm (see Figure S3) and for SEtIm at 11.92, 7.55, 7.13, 6.90, and 4.38 ppm (see Figure S6). These peak shifts were reproduced over several syntheses and are real. In addition, a broad band is observed in the far-IR spectrum for each [4Fe–4S] cluster. This feature is attributable to Fe–S vibrations, and it shifts with the substitution of the unique thiolato ligand. The precursor cluster $(Bu_4N)_2[Fe_4S_4(TriS)(SEt)]$ shows this vibration band at 344 cm^{-1}, which shifts to 339 cm^{-1} for the less rigid SEtIm ligand and to 349 cm^{-1} for the SPy ligand. Finally, the mass of the parent ions is observed by liquid chromatography time-of-flight mass spectrometry (LCT-MS), which supports the presence of the specified bifunctional thiolato ligands in these new clusters.

The new, site-differentiated $[Fe_4S_4]^{2+}$ clusters exhibit a shift of the first reduction potential, which yields the corresponding $[Fe_4S_4]^{+}$ species, to more positive values: the precursor cluster $(Bu_4N)_2[Fe_4S_4(TriS)(SEt)]$[14] and the phenylthiolate cluster $(Ph_4P)_2[Fe_4S_4(TriS)(SPh)]$[13] are reduced at –1026 and –894 mV [vs standard hydrogen electrode (NHE), in CH_2Cl_2], respectively. With the substitution of the pyridylthiolate and imidazolylthiolate ligands, the reduction is observed at more positive potentials of –746 and

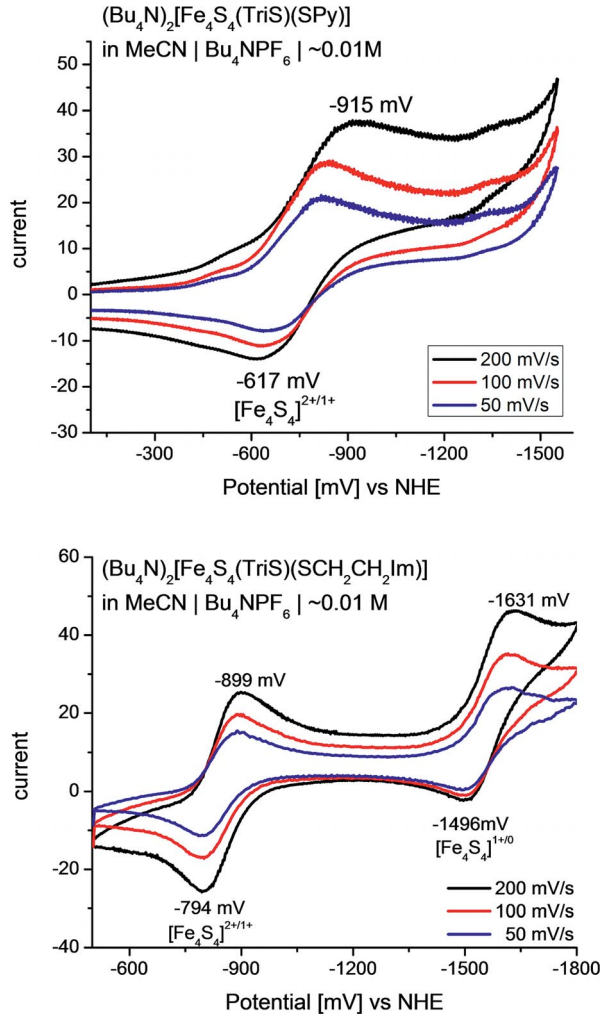

Figure 1. Cyclovoltammetry of $(Bu_4N)_2[Fe_4S_4(TriS)(SPy)]$ (top) and $(Bu_4N)_2[Fe_4S_4(TriS)(SEtIm)]$ (bottom) in MeCN.

–843 mV, respectively, as shown in Figure 1. This is likely due to the reduced electron density of these less electron-rich ligands, which is similarly seen for the phenylthiolate cluster in comparison to the ethylthiolate cluster. Note that the Fe^{III}/Fe^{II} reduction potential for iron porphyrins is observed in the range –200 to –300 mV. These potentials are suitable for an electron transfer path from the iron–sulfur cluster, which acts as the electron reservoir, to the heme that will bind the substrate for reduction. The generation of such a catalytic array consisting of a heme with a linked [4Fe–4S] cluster is the ultimate goal of this research.

Binding Affinities

It is essential that the metal moieties stay attached firmly in solution to use our proposed [Fe_4S_4]–heme constructs for catalysis. To gauge the binding affinity of the functionalized [4Fe–4S] cluster to different hemes, the corresponding zinc porphyrins were used for initial titrations because of their ease of preparation and their redox inactive property. In addition, four-coordinate zinc porphyrins bind only one axial ligand to generate five-coordinate complexes, and this process can be followed easily with absorption spectroscopy by monitoring a characteristic redshift of the Soret and Q bands of approximately 10 nm. Hence, binding constants can be obtained by simply following the change in absorption when the binding of an axial ligand to the four-coordinate zinc porphyrin occurs, which generates a five-coordinate species. These data can then be analyzed by using the Drago equation [Equation (1)], which is derived by using the Lambert–Beer law, to calculate the binding constant for the introduced ligand.[15]

$$K_{eq}^{-1} = \frac{A - A_i}{\varepsilon_{5C} - \varepsilon_{4C}} - [ZnP_i] - [B_i] + [ZnP_i][B_i]\frac{\varepsilon_{5C} - \varepsilon_{4C}}{A - A_i} \quad (1)$$

Here, K_{eq} is the binding constant calculated from the absorption data taken at a specific wavelength, A is the total absorption of the reaction mixture, A_i is the initial absorption, ε_{5C} and ε_{4C} are the extinction coefficients of the five-coordinate and four-coordinate zinc porphyrins, respectively, $[ZnP]_i$ is the initial concentration of the zinc porphyrin, and $[B]_i$ is the initial concentration of base. Thus, by independently determining the extinction coefficients of the four- and five-coordinate zinc porphyrins, by correcting the total concentration of the zinc porphyrin for dilution during the titration, and by recording the total concentration of base, the binding constant can be calculated. The titrations with the functionalized cubane clusters further required subtraction of the absorbance of the cubane cluster from the titration data to obtain accurate changes in absorption for the porphyrin signals. Additionally, the extinction coefficients of the five-coordinate zinc porphyrins with bound clusters are unknown, and therefore, they were assumed to be identical to those of the complexes [Zn(P)(MI)] and [Zn(P)(py)] (MI = 1-methylimidazole, py = pyridine) for $(Bu_4N)_2$[Zn(P)–{Fe_4S_4(TriS)(SEtIm)}] and $(Bu_4N)_2$-[Zn(P)–{Fe_4S_4(TriS)(SPy)}], respectively.

To compare binding affinities, MI and py, which are similar to SEtIm and SPy used in the clusters, were also titrated against the zinc porphyrins, and the binding constants were calculated. Table 1 includes all of the experimentally determined K_{eq} values for the titrations of zinc porphyrins, and two representative absorption plots for the titrations are included in Figure 2. The attained K_{eq} values were then used to recalculate the concentration of the five-coordinate zinc porphyrin–base complex and of the four-coordinate zinc porphyrin. The total absorbance for each titration point was calculated and plotted together with the experimental total absorbance against the molar equivalents of base added (Figure 2, insets). Overall, the calculated and the experimental absorbance match very well for the K_{eq} values determined here. The complete set of spectra is included in Figures S7, S8, and S9 in the Supporting Information.

Table 1. Binding constants of [Zn(P)] and an added base [M^{-1}].

Base	[Zn(TPP)]	[Zn(T*o*-F_2PP)]	[Zn(T*per*-F_5PP)]
Pyridine	5220	20300	77900
1-Methylimidizole	56800	204000	819000
$(Bu_4N)_2$[Fe_4S_4(TriS)(SPy)]	–[a]	7540	13200
$(Bu_4N)_2$[Fe_4S_4(TriS)(SEtIm)]	17100	26200	124000

[a] Titration not performed because of low binding affinity.

The increase in binding affinity of axial ligands for metalloporphyrins with electron-withdrawing groups at the ortho positions of the *meso*-phenyl substituents has been observed previously.[16] In these cases, it is thought that the electron density is drawn to the periphery of the porphyrin ring in the presence of the electron-withdrawing groups, which causes the porphyrin-ring nitrogen atoms to decrease in donicity, and in this way, the effective nuclear charge of the metal is increased. A strong σ-donor such as the N-donor ligands applied here will thus bind stronger to the open axial position in the fluorinated porphyrins. This trend is reproduced here: with an increasing number of electron-withdrawing fluorides present at the *meso*-phenyl rings, a distinct increase in the binding constant of base to the metalloporphyrins is observed. When pyridine is added to [Zn(TPP)], a binding constant of 5220 M^{-1} is determined for the formation of the five-coordinate complex [Zn(TPP)(py)]. This value matches well with the previously reported value of 6025 M^{-1} in benzene.[17] The analogous titrations with pyridine added to [Zn(T*o*-F_2PP)] [T*o*-F_2PP^{2-} = *meso*-tetra(*ortho*-difluorophenyl)porphyrin dianion] and [Zn(T*per*-F_5PP)] [T*per*-F_5PP^{2-} = *meso*-tetra(penta-fluorophenyl)porphyrin dianion] result in binding constants of 20300 and 77900 M^{-1}, respectively. Hence, a fourfold increase of the binding constant is observed upon going from [Zn(TPP)] to [Zn(T*o*-F_2PP)], which further increases fourfold in [Zn(T*per*-F_5PP)]. The same relative increase of the binding constant is observed for this series of zinc porphyrins when 1-methylimidazole is used as a base (see Table 1). Thus, both of the fluorinated metalloporphyrins are better options for obtaining heme–cluster adducts that are firmly attached in solution.

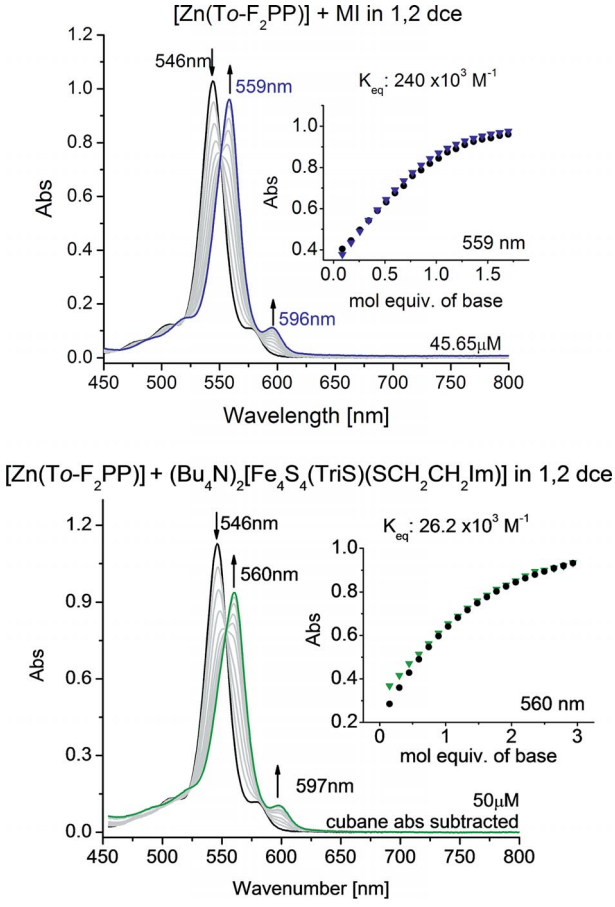

Figure 2. Absorption spectra for the titrations of [Zn(T*o*-F_2PP)] with 1-methylimidazole (top), including a comparison plot of the total experimental absorption (▼) vs. the total absorption (●) calculated from the derived K_{eq} value (inset), and with $(Bu_4N)_2[Fe_4S_4$(TriS)(SEtIm)] (bottom), including a comparison plot of the total experimental absorption (▼) vs the total absorption (●) calculated from the derived K_{eq} value (inset). Both experiments were conducted in 1,2-dichloroethane.

When the binding constants determined for pyridine and 1-methylimidazole for the same zinc porphyrin are compared, the value for the imidazole ligand is always higher by an order of magnitude. [Zn(TPP)] binding with py and MI affords binding constants of 5200 and 56800 M^{-1}, respectively. For [Zn(T*o*-F_2PP)], the binding constants for py and MI are 20300 and 204000 M^{-1}, respectively, and for [Zn(T*per*-F_5PP)], the values for py and MI are 77900 and 819000 M^{-1}, respectively. Imidazole is a stronger base than pyridine and therefore facilitates an increase in binding affinity by forming a stronger σ-bond to the heme, which is evident from the binding constants determined here.

Similar trends are also observed for the thiopyridine- and thioethylimidazole-functionalized [4Fe–4S] clusters. For the addition of $(Bu_4N)_2[Fe_4S_4$(TriS)(SPy)] to [Zn(T*o*-F_2PP)] and [Zn(T*per*-F_5PP)], binding constants of 7540 and 13200 M^{-1}, respectively, were determined. A distinct increase in binding affinity is also found when $(Bu_4N)_2[Fe_4S_4$(TriS)(SEtIm)] is used: for [Zn(TPP)], [Zn(T*o*-F_2PP)], and [Zn(T*per*-F_5PP)] increasing binding constants of 17100, 26200, and 124000 M^{-1}, respectively, were obtained along this series of zinc porphyrins. This corresponds to an increase in K_{eq} of 1.5 and 7.3 relative to [Zn(TPP)]. Likewise, the increased binding affinity for the imidazole-equipped cluster compared to the pyridine-containing cluster is apparent from the determined binding constants.

Unfortunately, the binding constants decrease strongly for the pyridine- and imidazole-bound cluster compared to the corresponding free ligands. For example, a comparison of the binding constants for py and $(Bu_4N)_2[Fe_4S_4$(TriS)(SPy)] to [Zn(T*o*-F_2PP)] shows a 2.6-fold decrease in the binding constant from 20300 to 7540 M^{-1}, respectively, for the cluster-bound pyridine ligand. Kirksey and co-workers have reported similar observations in the study of substituted pyridines binding to [Zn(TPP)], where the addition of deactivating groups to the pyridine decreases the binding constant.[17] For example, with [Zn(TPP)] in benzene, 4-cyanopyridine results in a K_{eq} value of 794 M^{-1} compared to 6025 M^{-1} for pyridine. One would expect that 4-thiopyridine would increase the binding constant, because thiols are activating groups. Thus, the observed decrease in the binding constant must be attributed to the electron-withdrawing, deactivating effect of the bound iron–sulfur cluster. Additionally, we believe that this decrease in K_{eq} for the pyridine- and imidazole-bound clusters is in part due to unfavorable steric interactions of these bulky ligands with the zinc porphyrins used here.

On the basis of our screening experiments, the largest binding constants are found for the imidazole-substituted cluster in combination with the fluorinated metalloporphyrins. Either fluorinated porphyrin is able to provide stable complexes in solution when the imidazole-functionalized cluster is used. However, the [M(T*per*-F_5PP)] metalloporphyrins have such a high solubility that isolating the heme–cluster adduct from solution by crystallization is likely difficult. Therefore, for these practical reasons, the [M(T*o*-F_2PP)] metalloporphyrins are most suitable for further large-scale preparations and spectroscopic investigations of the heme–cluster adducts. For example, for a typical reaction of [Zn(T*o*-F_2PP)] and $(Bu_4N)_2[Fe_4S_4$(TriS)(SEtIm)] at room temperature with heme and cluster concentrations of about 50 mM, the calculated ratio of bound to unbound complex is 97.3:1.

Cyclic Voltammetry of the Complete [4Fe–4S]–Heme Complex

An important property of the bound metalloporphyrin–iron–sulfur-cluster array is the ability to transfer electrons from the electron reservoir, the [4Fe–4S] cluster, to the heme. In the SIR and NIR enzymes, the [4Fe–4S] cluster is at a more negative reduction potential than the heme, as previously indicated (see Introduction). Additionally, the two metal centers are electronically coupled, which supports fast electron transfer through the sulfide bridge.[10,18] In our case, the complex of the [4Fe–4S] cluster and [Zn(T*o*-F_2PP)] does not contain a redox-active metal in the macro-

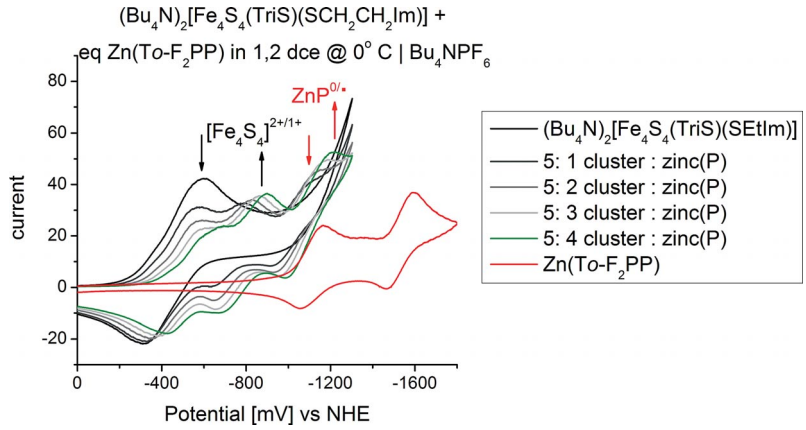

Figure 3. Cyclovoltammogram for the titration of 5 mM $(Bu_4N)_2[Fe_4S_4(TriS)(SEtIm)]$ with [Zn(To-F_2PP)] in 1,2-dichloroethane.

cycle for catalytic activity. Therefore, any reductions occurring at the metalloporphyrin are localized on the porphyrin ring. Individually, semi-reversible one-electron reduction events within the scanned potential range occur for the cluster at $E_{½}$ = –435 mV and for the zinc porphyrin at $E_{½}$ = –1110 mV in 1,2-dichloroethane (1,2-dce) (vs NHE). Interestingly, when an equivalent of zinc porphyrin is added (in one-fifth increments) to $(Bu_4N)_2[Fe_4S_4(TriS)(SEtIm)]$, the reduction event of the iron–sulfur cluster shifts more negative to –780 mV for a total difference in potential of 340 mV. The porphyrin-ring reduction does not change upon binding to the [4Fe–4S] cluster, as shown in Figure 3. In these experiments, the thiolate ligand remains bound to the [4Fe–4S] cluster in the absence of a donating solvent, as the loss of a ligand from the iron–sulfur cluster would result in decomposition of the cluster and subsequent precipitation. No precipitation was observed during any of the titration experiments, cyclic voltammetry experiments, or in bulk reaction mixtures.

Keeping in mind that the electronic coupling between the heme and the [4Fe–4S] cluster in our complexes is relatively weak compared to the sulfido-bridged SIR and NIR cofactor, the large negative shift in cluster potential observed upon heme binding must simply be due to the presence of the heme in close proximity to the cluster. It is in fact known that the first reduction of $(Bu_4N)_2[Fe_4S_4(TriS)(SEtIm)]$ strongly depends on the medium. For example, the redox potential in the polar, coordinating solvent acetonitrile is observed at –843 mV, as opposed to the less polar, non-coordinating solvent 1,2-dce, where this potential is –435 mV, as reported above, which is a remarkably large effect of the environment. Nature uses ferredoxins in a range of reduction potentials, which are highly tuned by the surrounding protein environment.[19] Likewise, the reduction potential of synthetic ferredoxins is tunable by the bound ligands, the electrolyte of the solution, and the polarity of the solvent.[20] Holm and co-workers reported the effect of various ligand substitutions at [4Fe–4S] clusters on reduction potentials. A substantial positive shift in the reduction potential of 90 mV is reported for their site-differentiated cluster, when the unique ligand SPh^- is substituted for $[SPh\text{-}p\text{-}NO_2]^-$, which results in reduction potentials of –1,060 and –970 mV (vs NHE), respectively.[20] Thus, the presence of strongly electron-withdrawing groups at the unique ligand can cause a positive shift in the reduction potential for the $[Fe_4S_4]^{2+}/[Fe_4S_4]^{1+}$ event. Interestingly, a titration of the functionalized site-differentiated [4Fe–4S] cluster with [Zn(To-F_2PP)] in 1,2-dce causes a shift of the reduction potential of the cluster to the negative range (see Figure 3), closer to the value found for MeCN. Because the coupling between the heme and the cluster across the S–CH_2–CH_2–Im bridge is likely weak, this implies an increase of the polarity of the cluster environment upon heme binding, which would then be responsible for the shift in the redox potential of the cluster.

Bulk-Scale Reactions

The synthesis of the bound complex $(Bu_4N)_2$[Zn(To-F_2PP)–{Fe_4S_4(TriS)(SEtIm)}] on a large scale for the purpose of isolating bound material and growing crystals for structure determination by X-ray crystallography was repeatedly attempted at concentrations >50 mM. Thus, at these concentrations, more than 97% of the bound complex is produced in solution. Absorption spectra of these solutions clearly indicate that the heme–cluster complex is formed under these conditions, as indicated by shifts of the Q bands of the metalloporphyrin. IR spectra further confirm that both [Zn(To-F_2PP)] and the iron–sulfur cluster are present in precipitated solids isolated from these reaction mixtures. Our efforts are continuing to finally attain a crystal structure of the complete catalytic array.

Summary

In this study, we report the preparation of the components for a linked catalytic array consisting of a metalloporphyrin and a functionalized site-differentiated [4Fe–4S] cluster, utilizing bridging ligands to connect these units. These bifunctional bridges contain a thiolate for preferential binding to the [4Fe–4S] cluster and an N-donor ligand

for binding to the axial position of the heme. Two new, site-differentiated [4Fe–4S] clusters with bound pyridine and imidazole linkers are reported in this study. A screening of the binding affinities of these pyridine- and imidazole-functionalized clusters to different zinc porphyrins indicates that imidazoles provide a stronger σ bond, which results in distinctively higher binding constants. Electron-withdrawing substituents added at the *meso*-phenyl groups of tetraphenylporphyrin (TPP^{2-}) further increase the binding constant of the base. Excitingly, *these results demonstrate the formation of the linked [4Fe–4S]–heme catalytic array in solution with high specificity*. Because of the high solubility of [M(T*per*-F_5PP)], [M(T*o*-F_2PP)] is the most suitable metalloporphyrin in combination with $(Bu_4N)_2[Fe_4S_4(TriS)(SEtIm)]$ for future spectroscopic studies and reactivity tests of the linked system. The binding between the chosen complexes was further confirmed by cyclic voltammetry. A significant influence of the solvent environment on the reduction potential of the [4Fe–4S] cluster was observed, and correspondingly, the binding of $(Bu_4N)_2[Fe_4S_4(TriS)(SEtIm)]$ to a zinc porphyrin causes a distinct shift in the reduction potential of the cluster, because the presence of the metalloporphyrin increases the polarity of the cluster environment. These results again confirm the formation of heme–cluster arrays in solution with our bridging ligands. At this point in time, a crystal structure has not been obtained for the bound complex. Importantly, our new complex design allows for individual component modifications to optimize the binding between the electron reservoir and the catalytic heme component. The continuation of this research is directed toward utilizing a redox-active iron porphyrin instead of a zinc porphyrin to create a catalytic site next to the iron–sulfur cluster.

Experimental Section

General Procedures: All cluster and ferrous heme syntheses were performed under a nitrogen atmosphere in a glove box or by utilizing common Schlenk-line techniques. ^{1}H and ^{19}F NMR spectra were acquired with a Varian MR400 400 MHz spectrometer and referenced to the solvent. Mid-IR spectra were collected with a Perkin–Elmer Spectrum BX FT-IR spectrometer, and far-IR data were obtained with a Nicolet 740 FT-IR spectrometer in KBr pellets. Mass spectrometric data were collected with a Micromass LCT time-of-flight mass spectrometer. Elemental analyses were performed by Atlantic Mircolab, Inc., Norcross, GA. Electronic spectra were measured with a Varian CARY 1E UV/Vis spectrometer. Cyclic voltammetry experiments were conducted in a 0.1 M solution of Bu_4NPF_6 in acetonitrile (MeCN) or 1,2-dichloroethane (1,2-dce) with a glassy-carbon working electrode, a Pt counter electrode, and a Ag/AgCl reference electrode with a EG&G Princeton Potentiostat/Galvanostat model 263A. The redox potentials are calibrated to the ferrocen–ferrocenium couple (Fc/Fc^+) and reported versus NHE.

Materials: All solvents were purified by distillation and degassed. All reagents were used as purchased and degassed under vacuum as needed, including pyridine and 1-methylimidazole. The compounds $TriSH_3$,[13,14,21] $1\text{-ImCH}_2\text{CH}_2\text{SH}$,[22] [Zn(TPP)],[23] [Zn(T*o*-F_2PP)],[24] [Zn(T*per*-F_5PP)],[25] [Fe(T*o*-F_2PP)],[26] and $(Bu_4N)_2[Fe_4S_4(SEt)_4]$[12] were prepared according to published procedures.

Synthesis of $(Bu_4N)_2[Fe_4S_4(TriS)(SEt)]$:[14] $(Bu_4N)_2[Fe_4S_4(SEt)_4]$ (0.87 g, 0.88 mmol) was dissolved in MeCN (50 mL) and stirred in a glove box. A solution of $TriSH_3$ (0.57 g, 0.88 mmol) in thf (5 mL) was prepared separately. Upon addition of the $TriSH_3$ solution to the stirred cubane solution, the color changed from brown-black to purple-black. The reaction flask was sealed, evacuated, and the mixture stirred for 4 h under a static vacuum. The dark purple solution was filtered with vacuum suction, and a dynamic vacuum was applied to the filtrate for a minute. The filtrate was taken to dryness, and the resulting black residue was dispersed in thf, filtered, and washed with thf until the filtrate ran clear. The thf filtrate was taken to dryness, and the black-purple residue was covered with Et_2O. The resulting purple-black solid was collected by suction filtration, washed with Et_2O (5–10 mL), and dried under vacuum to yield the desired product (0.78 g, 63% yield). ^{1}H NMR (400 MHz, CD_3CN, room temp.): δ = 13.08 (broad s, 2 H, SCH_2CH_3), 7.84 (broad d, 3 H, indolyl H), 7.72 (d, 3 H, indolyl H), 7.31 (t, 3 H, indolyl H), 6.96 (broad t, 3 H, indolyl H), 6.50 (s, 6 H, NCH_2), 3.06 (broad m, 16 H, Bu_4N^+), 2.43–2.09 (broad m, SCH_2CH_3 and Bz CH_2CH_3 9 H), 1.62 (broad m, 16 H, Bu_4N^+), 1.36 (broad m, 16 H, Bu_4N^+), 1.19 (broad m, 9 H, Bz CH_2CH_3), 0.97 (broad m, 24 H, Bu_4N^+) ppm. FT-IR (KBr): $\tilde{\nu}$ = 2958 (s), 2870 (s), 1608 (m), 1456 (s), 1379 (m), 1333 (m), 1294 (m), 1206 (m), 1151 (m), 1065 (m), 1010 (m), 880 (m), 739 (s), 645 (w), 426 (w), 344 (w) cm^{-1}.

Synthesis of $(Bu_4N)_2[Fe_4S_4(TriS)(SPy)]$: $(Bu_4N)_2[Fe_4S_4(TriS)(SEt)]$ (0.5 g, 0.325 mmol) was dissolved in MeCN (20 mL), and a solution of *p*-thiopyridine (0.040 g, 0.325 mmol) in MeCN (5 mL) was added with stirring in a glove box. The reaction vessel was sealed, and a vacuum was applied. The reaction mixture was stirred for 3 h under a static vacuum. The reaction mixture was filtered, and the filtrate was layered with Et_2O (100 mL). The black precipitate was collected by vacuum filtration, washed with diethyl ether, and dried under vacuum to yield a black, solid product (0.3 g, 58% yield). ^{1}H NMR (400 MHz, CD_3CN, room temp.): δ(TriS) = 7.88 (broad s), 7.73 (d), 7.31 (t), 6.98 (s), 6.59 (s), 2.42 (broad s), 1.36 (s) ppm; δ(SPy) = 8.83 (s), 6.1 (very broad) ppm; $\delta(Bu_4N^+)$ = 3.07, 1.93, 1.36, 0.96 (see Figure S3) ppm. FT-IR (KBr): $\tilde{\nu}$ = 2957 (s), 2869 (s), 1588 (m), 1567 (m), 1456 (s), 1378 (m), 1333 (m), 1293 (m), 1211 (m), 1150 (m), 1102 (m), 1061 (m), 1010 (m), 880 (m), 805 (m), 738 (s), 704 (m), 645 (w), 497 (w), 424 (w), 349 (w) (see Figure S2) cm^{-1}. UV/Vis (1,2-dce, λ in nm): 243 (sh), 283 (sh), 329 (sh), 522 (ε = 6160 $M^{-1}cm^{-1}$) (see Figure S1). CV (MeCN, 0.01 M): –746 mV $\{[Fe_4S_4]^{2+}/[Fe_4S_4]^{1+}\}$. LCT-MS (ESI+): *m*/*z* = 242 $(Bu_4N)^+$; LCT-MS (ESI–): *m*/*z* = 1346.1 $[(Bu_4N)\{Fe_4S_4(TriS)(SPy)\}]^-$, 1103.8 $[Fe_4S_4(TriS)(SPy)]^-$, 993.7 $[Fe_4S_4(TriS)]^-$.

Synthesis of $(Bu_4N)_2[Fe_4S_4(TriS)(SEtIm)]$: $(Bu_4N)_2[Fe_4S_4(TriS)(SEt)]$ (1.00 g, 0.65 mmol) was dissolved in MeCN (70 mL), and a solution of 1-thioethylimidazole (0.132 g, 0.71 mmol) in MeCN (5 mL) was added with stirring in a glove box. The reaction vessel was sealed, and a vacuum was applied. The reaction mixture was stirred for 4 h under a static vacuum. The reaction mixture was filtered, and the remaining solid was washed until the filtrate ran clear (<10 mL of MeCN). The filtrate was layered with Et_2O (250 mL). The black precipitate was collected by vacuum filtration, washed with diethyl ether, and dried under vacuum to yield a black, solid product (0.7 g, 67% yield). ^{1}H NMR (400 MHz, CD_3CN, room temp.): δ(TriS) = 7.83 (broad s), 7.72 (d), 7.30 (t), 6.95 (broad s), 6.52 (s), 2.41 (broad s), 1.18 (s) ppm; δ(SEtIm) = 11.92 (broad s), 7.55 (s), 7.13 (s), 6.90 (s), 4.38 (broad s) ppm; $\delta(Bu_4N^+)$ = 3.03, 1.58, 1.33, 0.94 (see Figure S6) ppm. FT-IR (KBr): $\tilde{\nu}$ = 2957 (s),

2929(s) 2869 (s), 1607 (w), 1454 (s), 1379 (m), 1339 (m), 1293 (m), 1209 (m), 1152 (m), 1106 (w), 1070 (w), 1009 (w), 881 (w), 738 (s), 653 (w), 528 (w), 426 (w), 339 (w) (see Figure S5) cm^{-1}. UV/Vis (1,2-dce, λ in nm): 333 (sh), 505 (ε = 7587 $M^{-1} cm^{-1}$) (see Figure S4). CV (MeCN, 0.01 M): –843 mV $\{[Fe_4S_4]^{2+}/[Fe_4S_4]^{1+}\}$ and –1563 mV $\{[Fe_4S_4]^{1+}/[Fe_4S_4]^{0}\}$; (1,2-dce, 0.005 M): –435 mV $[Fe_4S_4]^{2+}/[Fe_4S_4]^{1+}$. LCT-MS (ESI+): *m/z* = 242.1 $(Bu_4N)^+$; LCT-MS (ESI–) *m/z* = 1363.1 $[(Bu_4N)\{Fe_4S_4(TriS)(SEtIm)\}]^-$, 993.7 $[Fe_4S_4(TriS)]^-$, 560.4 $[Fe_4S_4(TriS)(SEtIm)]^{2-}$. $C_{76}H_{115}Fe_4N_7S_8$ (1606.7): calcd. C 56.81, H 7.21, N 6.10, S 15.97; found C 57.34, H 7.14, N 5.93, S 15.28.

UV/Vis Binding Constant Titrations: Stock solutions of the metalloporphyrins, 1-methylimidazole (MI), and pyridine (py) were prepared by utilizing an analytical scale for solids and a micro-syringe for liquids to load the reagents into volumetric flasks to afford stock solutions in the concentration range 1.00–15.0 mM in degassed 1,2-dichloroethane. A gas-tight quartz cuvette with a septa cap was filled with 1,2-dce (3 mL) dispensed through a burette. On the basis of the extinction coefficient of the Q band of the metalloporphyrin, the concentration of the stock solution was chosen accordingly to maintain the total absorbance below 1 for the titration reaction. An adequate amount of metalloporphyrin was added with a micro-syringe for a resulting concentration in the range 15–50 μM. To this solution was added an aliquot of base with a micro-syringe; the solution was shaken, and the absorption spectrum was recorded. These steps were repeated until the change in the absorbance of the Q band was negligible. For titrations where the base was a functionalized cubane cluster, analogous blank titrations were performed where 1,2-dce (3 mL) and the corresponding volume of pure solvent, equal to the volume of metalloporphyrin solution, were titrated with an identical volume of cubane solution for background subtraction. The concentrations of the metalloporphyrin and the base used for each titration are summarized in Table S1 in the Supporting Information.

Cyclovoltammetric Titrations: Stock solutions of [Zn(T*o*-F_2PP)] (14.9 mM) and $(Bu_4N)_2[Fe_4S_4(TriS)(SEtIm)]$ (25.0 mM) were prepared in a solution of Bu_4NF_6 (0.1 M) in 1,2-dce. Five solutions were prepared in volumetric flasks with increasing amounts of [Zn(T*o*-F_2PP)] by first adding 1 mL of the cubane stock solution and 0.33, 0.66, 1, 1.33, or 1.66 mL of the [Zn(T*o*-F_2PP)] stock solution. These solutions were then diluted to a total volume of 5 mL, which resulted in final concentrations of 5.0 mM for the cubane and 1.0, 2.0, 3.0, 3.9, and 4.9 mM for [Zn(T*o*-F_2PP)]. The Fc/Fc^+ couple was measured before and after each reaction mixture for external reference; potentials are reported versus NHE.

Supporting Information (see footnote on the first page of this article): UV/Vis absorption, IR, and ^1H NMR spectra of $(Bu_4N)_2[Fe_4S_4(TriS)(SPy)]$ and $(Bu_4N)_2[Fe_4S_4(TriS)(SEtIm)]$, table of binding titration conditions, and remaining titration plots for determining binding constants, as indicated in the text (Table 1).

Acknowledgments

D. L. G. acknowledges financial support from a University of Michigan Rackham Merit Fellowship. This work was supported by 3M (NTFG 5286067 to N. L.).

[1] R. Holm, P. Kennepohl, E. I. Solomon, *Chem. Rev.* **1996**, *96*, 2239–2314.
[2] Y. Nicolet, C. Piras, P. Legrand, C. E. Hatchikian, J. C. Fontecilla-Camps, *Structure* **1999**, *7*, 13–23.
[3] V. Svetlitchnyi, H. Dobbek, W. Meyer-Klaucke, B. T. Thomas Meins, P. Römer, R. Huber, O. Meyer, *Proc. Natl. Acad. Sci. USA* **2004**, *101*, 446–451.
[4] B. R. Crane, L. M. Siegel, E. D. Getzoff, *Science* **1995**, *270*, 59.
[5] M. E. Stroupe, E. D. Getzoff, in: *Handb. Metalloproteins* (Eds.: A. Messerschmidt, R. Huber, T. Poulos, K. Wieghardt), John Wiley & Sons, Chichester, UK, **2001**, p. 471–485.
[6] B. R. Crane, E. D. Getzoff, *Curr. Opin. Struct. Biol.* **1996**, *6*, 744.
[7] K. Parey, E. Warkentin, P. M. H. Kroneck, U. Ermler, *Biochemistry* **2010**, *49*, 8912–8921.
[8] K. W. Smith, M. E. Stroupe, *Biochemistry* **2012**, *51*, 9857–9868.
[9] L. J. Young, L. M. Siegel, *Biochemistry* **1988**, *27*, 4991–4999.
[10] P. A. Janick, L. M. Siegel, *Biochemistry* **1982**, *21*, 3538–3547.
[11] a) L. Cai, R. H. Holm, *J. Am. Chem. Soc.* **1994**, *116*, 7177–7188; b) C. Zhou, L. Cai, R. H. Holm, *Inorg. Chem.* **1996**, *35*, 2767–2772.
[12] B. A. Averill, T. Herskovitz, R. H. Holm, J. A. Ibers, *J. Am. Chem. Soc.* **1973**, *95*, 3523–3534.
[13] C. Walsdorff, W. Saak, S. Pohl, *J. Chem. Soc., Dalton Trans.* **1997**, 1857–1861.
[14] E. P. L. van der Geer, G. van Koten, R. J. M. Klein Gebbink, B. Hessen, *Inorg. Chem.* **2008**, *47*, 2849–2857.
[15] N. J. Rose, R. S. Drago, *J. Am. Chem. Soc.* **1959**, *81*, 6138–6141.
[16] a) F. A. Walker, U. Simonis, in: *Encycl. Inorg. Chem.* John Wiley & Sons, **2006**, p. 1–132; b) G. C. Vogel, B. A. Beckmann, *Inorg. Chem.* **1976**, *15*, 483–484; c) V. K. K. Praneeth, C. Näther, G. Peters, N. Lehnert, *Inorg. Chem.* **2006**, *45*, 2795–2811.
[17] C. H. Kirksey, P. Hambright, C. B. Storm, *Inorg. Chem.* **1969**, *8*, 2141–2144.
[18] J. A. Christner, E. Münck, P. A. Janick, L. M. Siegel, *J. Biol. Chem.* **1983**, *258*, 11147–11156.
[19] H. Beinert, R. H. Holm, E. Münck, *Science* **1997**, *277*, 653659.
[20] C. Zhou, J. W. Raebiger, B. M. Segal, R. H. Holm, *Inorg. Chim. Acta* **2000**, *300–302*, 892–902.
[21] A. Vacca, C. Nativi, M. Cacciarini, R. Pergoli, S. Roelens, *J. Am. Chem. Soc.* **2004**, *126*, 16456–16465.
[22] C. A. M. Afonso, N. M. T. Lourenço, A. de A. Rosatella, *Molecules* **2006**, *11*, 81–102.
[23] a) A. D. Adler, F. R. Longo, J. D. Finarelli, J. Goldmacher, J. Assour, L. Korsakoff, *J. Org. Chem.* **1967**, *32*, 476–476; b) T. P. Wijesekera, D. A. Dolphin, in: *Metalloporphyrins in Catalytic Oxidations* (Ed.: R. A. Sheldon), Ed. M. Dekker, New York, NY, **1994**, p. 193–239.
[24] J. S. Lindsay, R. W. Wagner, *J. Org. Chem.* **1989**, *54*, 828–836.
[25] H. Quast, T. Dietz, A. Witzel, *Liebigs Ann.* **1995**, 1495–1501.
[26] R. A. Ghiladi, R. M. Kretzer, I. Guzei, A. L. Rheingold, Y.-M. Neuhold, K. R. Hatwell, A. D. Zuberbu, K. D. Karlin, *Inorg. Chem.* **2001**, *40*, 5754–5767.

Received: March 6, 2013
Published Online: June 17, 2013

